Mounting a Water Vapor Radiometer on a DSN Antenna Subreflector: Benefits for Radio Science and Millimeter-Wavelength VLBI

R. Linfield[1]

Mounting a water vapor radiometer (WVR) on the back of a DSN antenna subreflector would allow calibration of delay fluctuations on timescales of 10–100 s, which is not possible with the current generation of off-axis WVRs. This calibration would improve the accuracy of short-timescale radio science experiments with planetary spacecraft. It would greatly improve the coherence of 86-GHz very long baseline interferometry (VLBI), allowing detection of substantially weaker sources, and giving much better amplitude calibration (i.e., higher dynamic range images).

Numerical calculations have quantified the expected performance for both radio science and mm-VLBI applications as a function of elevation angle and WVR beamwidth. A beamwidth, full width at half maximum (FWHM), of 2 deg would allow useful calibration capability. However, FWHM $\approx$ 1 deg is needed for optimum performance.

I. Introduction

A. Effects of Tropospheric Fluctuations

Radio signals propagating through the Earth's atmosphere will have their phase corrupted by irregularities in the index of refraction. The contribution of charged particles in the ionosphere and interplanetary medium to the phase of the signal scales as ν^{-1}, as compared to ν^{+1} for the neutral troposphere (ν is the radio frequency). Above 3–8 GHz, density fluctuations in the neutral troposphere produce the dominant contributions to the total phase fluctuations.

Radio science experiments that involve signal propagation between Earth and a spacecraft will be affected by these phase fluctuations. For experiments such as gravitational wave searches [1], the accuracy of the desired measurements is likely to be limited by the fluctuations.

---

[1] Astrophysics Science Centers.

The research described in this publication was carried out by the Jet Propulsion Laboratory, California Institute of Technology, under a contract with the National Aeronautics and Space Administration.

Very long baseline interferometry (VLBI) involves simultaneous observations of a celestial radio source with two or more radio telescopes. The phase stability of the hydrogen maser frequency standards used in VLBI is sufficiently good that the coherence times of observations are limited by the phase fluctuations in the local medium (the Earth's troposphere at high radio frequencies). The coherence time decreases rapidly toward higher observing frequency, and is often only 10–30 s at 86 GHz [2], a frequency at which the DSS-13 antenna may be usable for observations. VLBI observations require that a source (either the target object or an angularly nearby calibrator) be detectable within one coherence time. The short coherence times at 86 GHz and above (millimeter wavelengths) result in poor sensitivity for VLBI at these frequencies.

B. Calibration with Water Vapor Radiometers

At radio frequencies, the refractivity of water vapor is roughly 20 times larger than for dry air [3,4]. Because of its high refractivity and inhomogeneous distribution in the atmosphere, water vapor is responsible for most of the tropospheric refractivity fluctuations.

Water vapor radiometers (WVRs) [5] measure the thermal emission from tropospheric water vapor along a specific line of sight on the sky. These measurements can then be used to infer the time-variable delay in the same direction, potentially improving the accuracy of radio science measurements and the coherence of high-frequency VLBI [6].

A high-performance WVR-based troposphere calibration system has been designed and built at JPL in support of radio science measurements with the Cassini spacecraft [7,8]. As a test of the accuracy of this system, phase fluctuations measured with radio interferometry over a 21-km baseline at Goldstone were successfully calibrated [9].

The Cassini troposphere calibration system was designed to optimize calibration of fluctuations on timescales of 100–10,000 s, with performance at 1000–10,000 s given the highest priority. Because of the timescales of interest, the WVR in this system will be located on the ground, approximately 50 m from the axis of the DSN antenna used for the radio link between Earth and Cassini. The weight of the radiometer is 68 kg, and the weight of its clear-aperture, off-axis parabolic antenna is 27 kg. Minimizing the weight was not a primary consideration in the design of the system.[2]

The offset location of the WVR causes its sampled troposphere volume to be different (little or no overlap) from the volume traversed between the spacecraft and the DSN antenna. As a result, accurate calibration of fluctuations on short timescales (<100 s) is not possible [10]. A different WVR location is needed for calibration of short-timescale radio science measurements or mm-wavelength VLBI.

The volume mismatch can be eliminated by integrating a WVR into a beam-waveguide (BWG) antenna. Tests of such a configuration have been encouraging [11]. However, there will be significant challenges in designing such a system, especially the difficulty of splitting the three WVR frequencies from the signals used for the spacecraft uplink and downlink. Such a splitting must be extremely stable in terms of amplitude loss and added noise. It is worthwhile considering other WVR configurations.

The configuration analyzed in this article consists of a WVR mounted on the back of a DSN subreflector, as illustrated schematically in Fig. 1. The WVR would have a conical beam that is coaxial with the cylindrical near-field beam of the DSN antenna. Because of the substantial overlap between the cylindrical and conical troposphere volumes sampled by the DSN antenna and WVR, the volume mismatch can be much smaller than for an offset beam. As with an offset location, a WVR on the back of a DSN subreflector can use a clear-aperture reflector to minimize sidelobes. This location avoids two of the problems with an integrated BWG location: scattering off the DSN antenna feed legs (causing

[2] A. Tanner, personal communication, Jet Propulsion Laboratory, Pasadena, California, March 19, 2001.

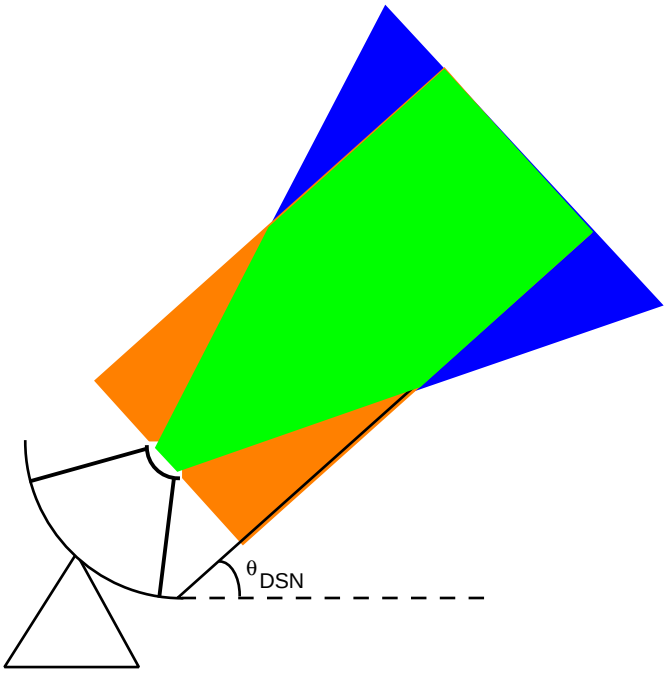

Fig. 1. Geometry of the WVR configuration studied in this article. The DSN antenna samples a cylindrical volume. The WVR samples a truncated conical volume. The orange volume is sampled only by the DSN antenna. The blue volume is sampled only by the WVR. The green volume is sampled by both.

time-variable ground pickup) and the complication of splitting the signal between the radio science and WVR frequencies.

The drawbacks of this subreflector location are (1) it does not completely eliminate the volume mismatch problem, (2) the WVR must have low weight to avoid causing excess flexure of the feed legs, and (3) access to the WVR for maintenance is not as convenient as for an offset location.

II. Fluctuation Model and Calculations

A. Basic Turbulence Model

The refractivity fluctuations were assumed to have a Kolmogorov spectrum, with uniform turbulence strength from the surface to a height of 2 km. The fluctuation level was assumed to be zero above 2 km, which is the mean scale height of the wet troposphere. A refractivity structure constant, C_n, of 1.1×10^{-7} m$^{-1/3}$ was used; this and a turbulent slab height of 2 km reproduces the mean conditions at the three DSN sites.[3] The scaling to other levels of turbulence is discussed in Section III (for Allan Deviation, the scaling is linear in C_n).

A frozen flow model (the Taylor hypothesis) was used to relate spatial and temporal fluctuations, using a constant wind velocity $\vec{v}_w$. Calculations were performed as in [10] and [12].

B. Conical–Cylindrical Mismatch

The volume of wet troposphere sampled by the DSN antenna was modeled as a cylinder of radius $r_{\rm DSN}$ and length $h/\sin\theta_{\rm DSN}$, where h is the thickness of the turbulent layer (2 km) and $\theta_{\rm DSN}$ is the elevation

[3] R. Treuhaft, personal communication, Jet Propulsion Laboratory, Pasadena, California, 2001.

angle of the antenna. The center of the base of the cylinder was defined as the coordinate system origin, and the pointing direction was in the x–z plane (the region of tropospheric fluctuations was slightly expanded to include the "corners" of the cylinder that were below $z = 0$ or above $z = 2$ km). The wet tropospheric delay seen by the DSN antenna was then

$$\left.\begin{aligned} \tau_{\rm DSN}(t) &= \frac{1}{\pi r_{\rm DSN}^2 \sin\theta_{\rm DSN}} \int_0^{2\pi} d\omega \int_0^{r_{\rm DSN}} R dr \int_0^{h} N[\vec{r}_{\rm DSN}(\theta_{\rm DSN}, R, \omega, z_0) + \vec{v}_w t] dz_0 \\ \vec{r}_{\rm DSN}(\theta_{\rm DSN}, R, \omega, z_0) &= \begin{pmatrix} z_0 \cot\theta_{\rm DSN} - R\cos\omega\sin\theta_{\rm DSN} \\ R\sin\omega \\ z_0 + R\cos\omega\cos\theta_{\rm DSN} \end{pmatrix} \end{aligned}\right\} \quad (1)$$

where N is the refractivity. The volume of wet troposphere sampled by the WVR was modeled as a truncated cone, whose axis was coincident with the DSN antenna axis. The truncation (with a diameter of 2 m) gave a slightly more realistic treatment of the beam of a WVR like the one used for the Cassini troposphere calibration system. More importantly, removing a small region at the apex of the cone significantly speeded up convergence of the numerical integrations. All derivatives of the refractivity structure function become infinite at zero separations, so very small physical separations in the numerical integration routines introduce relatively large numerical errors. The length of the axis of the truncated cone was $h/\sin\theta_{\rm DSN}$. A Gaussian beam profile was used, truncated (for numerical convenience) at a diameter 3.4 times the full width at half maximum (FWHM) of the Gaussian profile. The center of the WVR antenna was at the coordinate system origin. In practice, there would be an extra path length $\sim 2r_{\rm DSN}$ in the volume sampled by the DSN antenna, but this extra volume is small compared to the total tropospheric path length. The wet tropospheric delay seen by the WVR is

$$\left.\begin{aligned} \tau_{\rm WVR}(t) &= \frac{1}{\Omega_{\rm WVR}} \int_0^{2\pi} d\omega \int_0^{\psi_{\max}} \frac{W(u)\sin(u)}{\sin\theta(u,\omega)} du \int_{h_{\min(u,\omega)}}^{h_{\max(u,\omega)}} N[\vec{r}_{\rm WVR}(\theta,\phi,z) + \vec{v}_w t] dz \\ \vec{r}_{\rm WVR}(\theta,\phi,z) &= \begin{pmatrix} -d_{\rm WVR}\cos\theta_{\rm DSN} + [z + d_{\rm WVR}\sin\theta_{\rm DSN}]\cot\theta\cos\phi \\ [z + d_{\rm WVR}\sin\theta_{\rm DSN}]\cot\theta\sin\phi \\ z \end{pmatrix} \end{aligned}\right\} \quad (2)$$

Here $\Omega_{\rm WVR}$ is the solid angle of the Gaussian WVR beam, which is truncated at an angular radius $\psi_{\max}$; $W(u)$ is the amplitude (weight) of the beam profile an angle u from the axis; and $\theta(u,\omega)$ and $\phi(u,\omega)$ are the elevation angle and azimuth for rays originating at location (u,ω) in the beam. Also, $d_{\rm WVR}$ is the length (along its axis) of the truncated section of the cone; N is the refractivity; and $\vec{v}_w$ is the wind velocity.

The error (uncalibrated residual) after subtracting the WVR delay from the DSN delay will be

$$\tau_{\rm err}(t) \equiv \tau_{\rm DSN}(t) - \tau_{\rm WVR}(t) \quad (3)$$

In order to derive the expected Allan Deviation [14] and coherence, we first must calculate the delay structure function:

$$
\begin{aligned}
D_\tau(\Delta t) \equiv & \left\langle \left[\tau_{\rm err}(t+\Delta t) - \tau_{\rm err}(t)\right]^2 \right\rangle \\
& = 2\left\langle \tau^2_{\rm DSN}(t)\right\rangle - 2\big\langle \tau_{\rm DSN}(t+\Delta t)\tau_{\rm DSN}(t)\big\rangle + 2\left\langle \tau^2_{\rm WVR}(t)\right\rangle \\
& \quad - 2\big\langle \tau_{\rm WVR}(t+\Delta t)\tau_{\rm WVR}(t)\big\rangle - 4\big\langle \tau_{\rm DSN}(t)\tau_{\rm WVR}(t)\big\rangle \\
& \quad + 2\big\langle \tau_{\rm DSN}(t+\Delta t)\tau_{\rm WVR}(t)\big\rangle + 2\big\langle \tau_{\rm DSN}(t)\tau_{\rm WVR}(t+\Delta t)\big\rangle
\end{aligned} \tag{4}
$$

Here the angle brackets (<>) represent ensemble averages, or expectation value.

Substitution of Eqs. (1) and (2) into Eq. (4) leads to an expression for $D_\tau(\Delta t)$ (see [12] and [13] for details), consisting of six-dimensional integrals of the refractivity structure function $D_n(\Delta\vec{x})$:

$$
D_n(\Delta\vec{x}) = C_n^2 \left|\Delta\vec{x}\right|^{2/3} \tag{5}
$$

These integrals were evaluated numerically for all integer seconds up to 200 s. The majority of the central processing unit time was used for the shorter time intervals.

C. Allan Deviation

One measure of the power in $\tau_{\rm err}(t)$ at different timescales is Allan Deviation [14]. The Allan Variance $\sigma_y^2(\Delta t)$ of a delay process $\tau(t)$ is

$$
\sigma_y^2(\Delta t) \equiv \frac{\left\langle \left[\tau(t+2\Delta t) - 2\tau(t+\Delta t) + \tau(t)\right]^2 \right\rangle}{2(\Delta t)^2} \tag{6}
$$

A little algebra leads to

$$
\sigma_y(\Delta t) = \frac{1}{c\Delta t}\sqrt{2D_\tau(\Delta t) - \frac{1}{2}D_\tau(2\Delta t)} \tag{7}
$$

The factor of c (velocity of light) is needed when $D_\tau(\Delta t)$ is expressed in length^2 units, as in this article.

D. Coherence

The coherence Coh(T) of a delay process $\tau(t)$ at an observing frequency ν is [15]

$$
\left\langle {\rm Coh}^2(T)\right\rangle = \frac{2}{T}\int_0^T \left(1 - \frac{t'}{T}\right) e^{-2\pi^2\nu^2 D_\tau(t')/c^2} dt' \tag{8}
$$

(where $D_\tau(t)$ is expressed in length^2 units, as in the rest of this article). For VLBI, both telescopes of a baseline contribute to the coherence loss, with independent fluctuations on the timescales over which coherence loss occurs. We can account for the two telescopes in Eq. (8) by doubling the value of $D_\tau(\Delta t)$ from a single telescope.

E. Thermal WVR Noise

On short timescales, thermal noise from a WVR is important. With a Dicke-switched, gain-stabilized radiometer, the noise $N(t_{\rm int})$ in an integration time $t_{\rm int}$ is

$$N(t_{\rm int}) \approx \frac{2T_{\rm sys}}{\sqrt{\rm BW\ t_{\rm int}}} \tag{9}$$

For the main vapor-sensing frequency channel of 20.7 or 23.8 GHz, a 1-K brightness temperature corresponds to ≈6 mm of path delay. Expressing $N(t_{\rm int})$ in units of path delay, we get

$$N(t_{\rm int}) = \frac{0.012\ T_{100}}{{\rm BW}_{100}^{0.5} t_{\rm int_s}^{0.5}}\ {\rm cm} \tag{10}$$

Here T_{100} is the system temperature in units of 100 K; ${\rm BW}_{100}$ is the detected bandwidth in units of 100 MHz; and $t_{\rm int_s}$ is the integration time in seconds.

An optimistic lower bound to the WVR thermal noise contributions to the Allan Deviation comes from setting $\Delta t = t_{\rm int}$ (we lose all information on timescales shorter than Δt), BW = 400 MHz, and system temperatures of 300 K (uncooled amplifier) or 60 K (cryogenic amplifier). (For comparison, the total system temperature for the Cassini troposphere calibration system WVR is ≈600 K). The contribution of thermal noise to the Allan Deviation is $\sigma_y(\Delta t) = N(t_{\rm int})\sqrt{3}/(c\Delta t)$, or

$$\sigma_y(\Delta t) = \frac{1.0 \times 10^{-12}}{\Delta t_s^{1.5}} \qquad \text{(WVR thermal noise, uncooled amplifier)} \tag{11}$$

$$\sigma_y(\Delta t) = \frac{2.1 \times 10^{-13}}{\Delta t_s^{1.5}} \qquad \text{(WVR thermal noise, cryogenic amplifier)} \tag{12}$$

WVRs operating at the 22-GHz water vapor line cannot do better than these limits. (At sites with very low water vapor column density, the 183-GHz water vapor line is optically thin; measurement at this frequency could give lower thermal noise in path delay units.)

The contribution of thermal WVR noise to the structure function for $\tau_{\rm err}$ for each DSN antenna is independent of Δt:

$$D_\tau(\Delta t) = 2N^2(t_{\rm int}) = \frac{2.9 \times 10^{-4}\ T_{100}^2}{{\rm BW}_{100} t_{\rm int_s}}\ {\rm cm}^2 \qquad \text{(WVR thermal noise)} \tag{13}$$

For the WVR parameters given above, and including an extra factor of 2 in the exponent in Eq. (8) for the effect of two WVRs, we get

$$4\pi^2\nu^2 D_\tau(\Delta t)/c^2 = \frac{0.21}{t_{\rm int_s}} \left(\frac{\nu}{86\ {\rm GHz}}\right)^2 \qquad \text{(thermal noise, uncooled WVR)}$$

$$= \frac{0.008}{t_{\rm int_s}} \left(\frac{\nu}{86\ {\rm GHz}}\right)^2 \qquad \text{(thermal noise, cryogenic WVR)} \tag{14}$$

With an integration time ≥5 s, the coherence loss will be minor at 86 GHz, even for an uncooled WVR. For VLBI observations at higher frequencies (probably not possible with any existing DSN antenna), cooled receivers or longer integration times would be needed to minimize coherence loss due to WVR noise.

III. Results

A. Allan Deviation

Figures 2 through 4 show the Allan Deviation for WVR beam sizes (FWHM) of 1 deg, 2 deg, and 4 deg for coaxial DSN and WVR beams. A 1-deg FWHM is about the smallest beamwidth that could

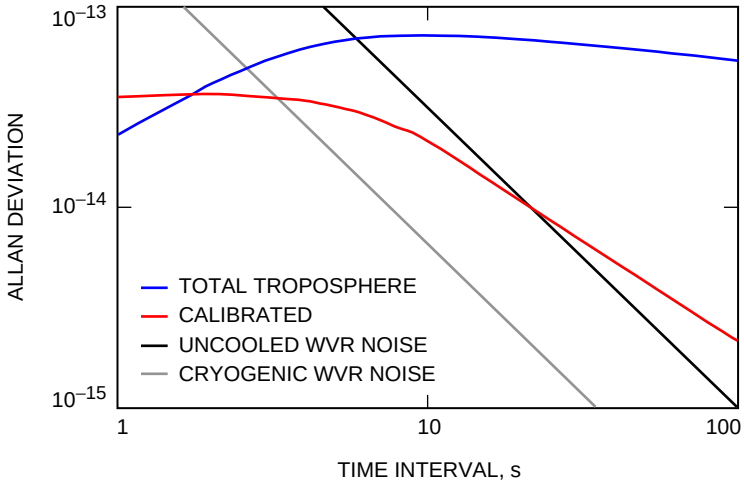

Fig. 2. Allan Deviation of troposphere fluctuations seen with a 34-m DSN antenna. The upper (blue) curve shows the total fluctuations; the lower (red) curve shows the residual after calibration with an ideal WVR having a 1-deg FWHM beam. The black and gray lines show the limits resulting from thermal WVR noise.

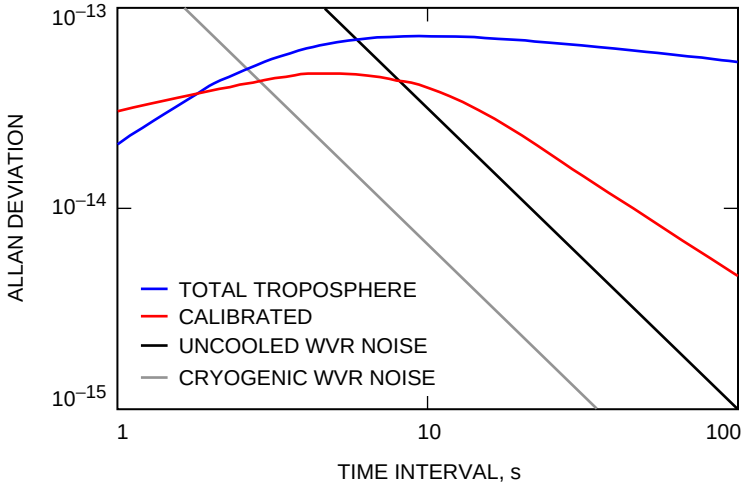

Fig. 3. Allan Deviation of troposphere fluctuations seen with a 34-m DSN antenna. The upper (blue) curve shows the total fluctuations; the lower (red) curve shows the residual after calibration with an ideal WVR having a 2-deg FWHM beam. The black and gray lines show the limits resulting from thermal WVR noise.

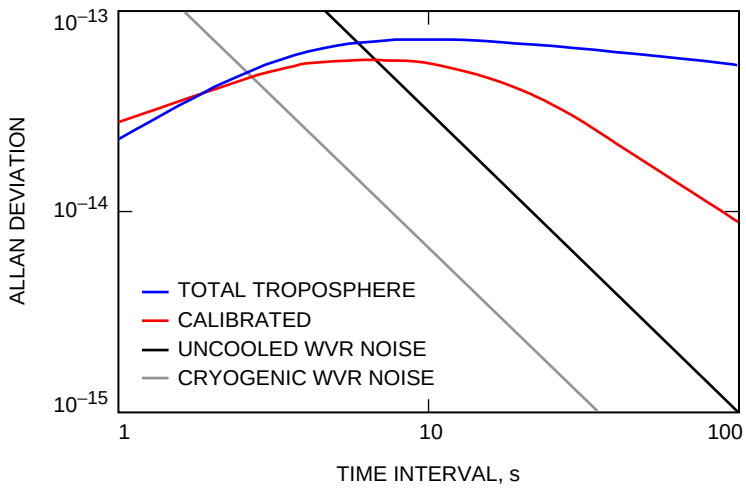

Fig. 4. Allan Deviation of troposphere fluctuations seen with a 34-m DSN antenna. The upper (blue) curve shows the total fluctuations; the lower (red) curve shows the residual after calibration with an ideal WVR having a 4-deg FWHM beam. The black and gray lines show the limits resulting from thermal WVR noise.

be achieved with an antenna that (1) could be mounted on the back of a DSN subreflector and (2) is underilluminated in order to achieve a very low sidelobe level. (For comparison, the Cassini troposphere calibration system WVR has an FWHM of approximately 1 deg). The elevation angle is 30 deg, and the antenna diameter is 34 m for the results shown in Figures 2 through 4. Both the total Allan Deviation seen by the DSN antenna and the Allan Deviation of the calibrated signal ($\tau_{\rm err}$) are shown. The thermal noise limits for uncooled [Eq. (11)] and cryogenic [Eq. (12)] WVRs are also plotted in each figure.

Figure 5 shows the dependence on elevation angle: $\theta_{\rm DSN}$ = 60 deg, 30 deg, and 20 deg for a 2 deg FWHM WVR beam. The mismatch error is smallest at high elevation angles, where the WVR beam has less chance to spread out before it reaches the top of the wet troposphere. At low elevation angles ($\leq$30 deg), there is a large benefit to reducing the beamwidth below FWHM = 2 deg.

Figure 6 shows the case of an offset WVR location for comparison: 50 m between the WVR and the DSN axis, 1-deg FWHM, and 30-deg elevation angle.

All these calculations used a wind velocity of 8 m/s for the turbulent layer, with an orientation 45 deg to the pointing direction of the DSN antenna.

All the Allan Deviation curves (total and calibrated) scale linearly with C_n; the ratio of the calibrated to total value will not change. If the wind velocity of the turbulent wet troposphere is different from 8 m/s, the amplitude of the total and calibrated Allan Deviation will not be affected. However, the time scale for both curves will change, inversely proportional to wind velocity (i.e., for a *larger* wind velocity, a given fluctuation level will occur on a *shorter* timescale). The thermal noise limits do not depend on C_n or wind velocity.

B. Coherence

Figure 7 shows the expected coherence for VLBI observations at 86 GHz, with and without WVR calibration. For this plot, the elevation angle was 20 deg; the wind was 8 m/s at azimuth 45 deg; and the structure constant was 1.5 times the DSN average (with multiple stations in a VLBI experiment, at least one is likely to have turbulent tropospheric conditions, and the elevation angle is usually low at some stations). The three panels in the figure are for WVR beam sizes (FWHM) of 1 deg, 2 deg, and 4 deg.

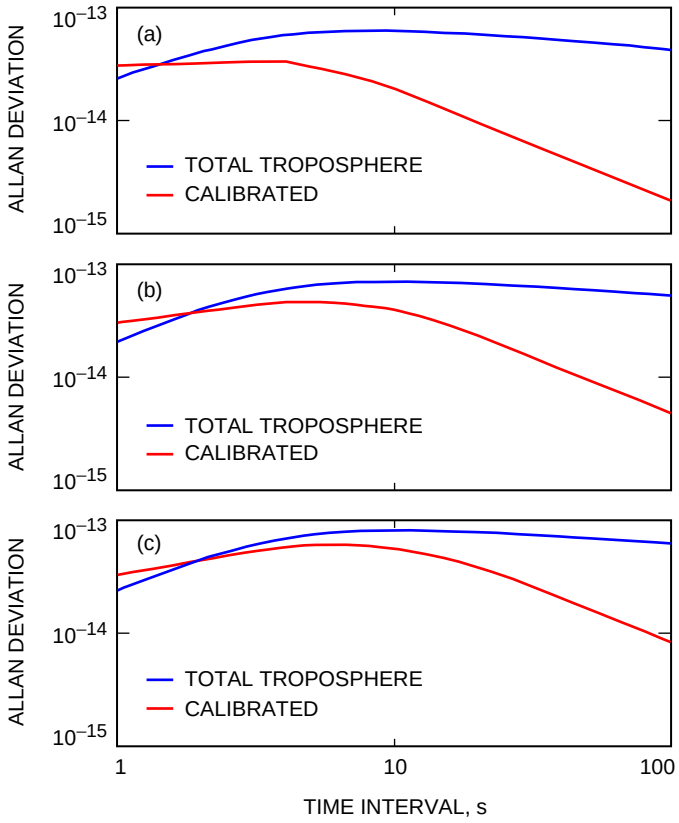

Fig. 5. Elevation-angle dependence of beam mismatch error, showing the total and calibrated (residual) fluctuations for a WVR with 2-deg FWHM, mounted on a 34-m-diameter DSN antenna, at elevation angles of (a) 60 deg, (b) 30 deg, and (c) 20 deg.

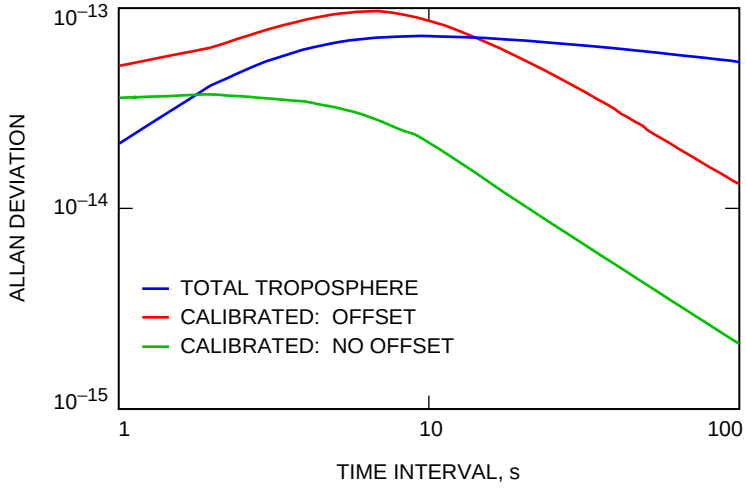

Fig. 6. The consequences of locating the WVR off the DSN antenna. The blue curve shows the total tropospheric fluctuations; the red curve shows the residual fluctuations after application of WVR calibration, with a 1-deg FWHM WVR beam, offset 50 m from the DSN antenna axis; and the green curve (from Fig. 2) shows the calibration capability if there were no offset (the WVR is on axis).

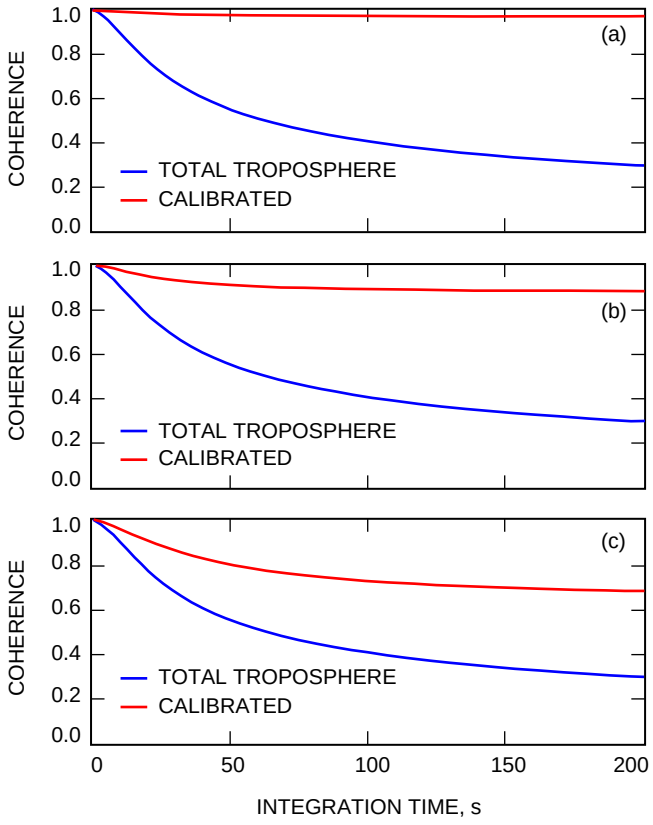

Fig. 7. Coherence improvements for 86-GHz VLBI, using an ideal WVR mounted on a DSN antenna subreflector, at a 20-deg elevation angle, for WVR beam sizes (FWHM) of (a) 1 deg, (b) 2 deg, and (c) 4 deg.

For comparison, Fig. 8 shows the coherence for a 50-m offset WVR location, a beam size of 1 deg, and an elevation angle of 20 deg.

For small coherence loss, $1 - \mathrm{Coh}$ is proportional to C_n^2, for both the calibrated and uncalibrated cases in Figs. 7 and 8. The timescale in both figures is inversely proportional to v_w, as for the Allan Deviation.

IV. Conclusion and Discussion

A. Radio Science Application

A WVR mounted on a DSN antenna subreflector could greatly reduce the beam mismatch problem of an off-axis WVR location. A 4-deg FWHM on-axis WVR gives slightly better performance than a narrow beam WVR located 50 m off axis (see Figs. 4 and 6). The performance improves quickly as the WVR beamwidth is reduced. Calibration with an on-axis 1-deg FWHM WVR could reduce the Allan Deviation of troposphere fluctuations by a factor of 3 at 10 s, and a factor of 20 at 100 s. Future radio science experiments could benefit from this performance if they use two-way tracking to eliminate dependence on onboard oscillator stability, or if they fly an advanced onboard oscillator that is more stable than the troposphere.

With an uncooled WVR, the total error (thermal noise plus beam mismatch) at $\Delta t \geq 10$ s continues to decrease as the WVR beam size decreases, down to 1-deg FWHM (see Figs. 2 through 4). Further

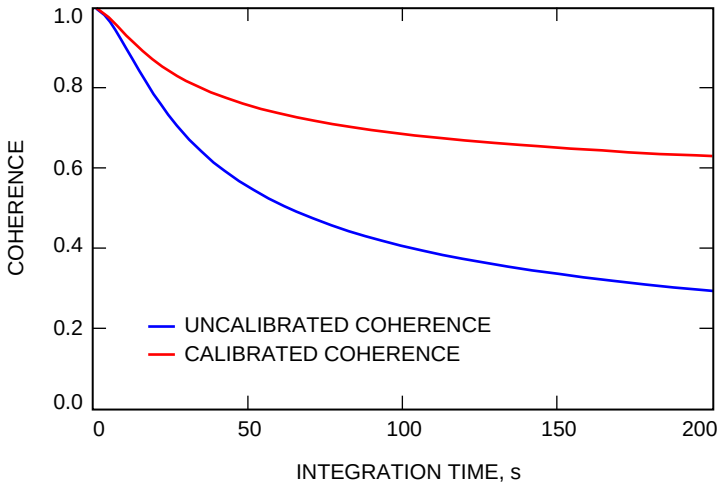

Fig. 8. Coherence improvement for 86-GHz VLBI, using an ideal WVR located 50 m from the axis of a DSN antenna, at a 20-deg elevation angle, with a WVR beam size of 1-deg FWHM.

reduction in WVR beam size, or integration into a BWG antenna, would not give better total performance with an uncooled WVR.

Conversely, changing from an uncooled to a cryogenic WVR would yield an improvement in total performance only for an on-axis WVR with FWHM <2 deg, or for a WVR integrated into a BWG antenna. For an integrated location (zero mismatch error) with a cryogenic WVR, thermal WVR noise sets a lower limit for useful calibration (improvement by a factor ≥3) of $\Delta t \approx 5$ s.

B. Coherence

An on-axis WVR could greatly improve the coherence of 86-GHz VLBI observations, at least during clear weather, when WVR measurements are not corrupted by clouds. The higher coherence would have two large benefits. First, the signal-to-noise ratio (SNR) is linearly proportional to the coherence, so calibration with a WVR would increase the SNR by a factor >2 and allow detection of weaker sources. Second, when the atmospheric coherence is low, it will also be highly variable (because atmospheric fluctuations vary in magnitude from one integration time to the next). This highly variable coherence leads to a large amplitude calibration uncertainty and large errors in the images obtained from interferometry. The coherence resulting from WVR calibration is close to 1.0. Therefore, the calibrated coherence would exhibit only mild variability, allowing better amplitude calibration and more accurate images of compact radio sources.

A beam size of 4 deg or an off-axis location would give some coherence improvement. However, the calibrated coherence would be a strong function of the fluctuation level (C_n) and the wind conditions, resulting in degraded science return. Therefore, an on-axis WVR with a beam size of 2-deg FWHM or smaller is needed, with a beam size near 1 deg desired for the best performance.

C. Cautions/Other Error Sources

Beam mismatch and WVR thermal noise are not the only error sources in WVR calibration. At the short timescales (<100 s) of interest in this analysis, retrieval errors [8] may be important. Of greater concern is the magnitude of dry delay fluctuations, which we currently have no idea how to calibrate. Fluctuations in the temperature and density of dry air on spatial scales of a few centimeters limit the angular resolution of optical telescopes. Extrapolating to the much larger spatial scales (tens to hundreds of meters) that correspond to timescales of 10–100 s is quite uncertain. Dry fluctuations could be as large

as ∼30 percent of the total fluctuation level. However, measurements in the near infrared [16] suggest that these fluctuations grow more slowly with spatial scale than simple Kolmogorov turbulence theory predicts, so the actual magnitude may be much less than this 30 percent level.

Acknowledgments

I thank A. Tanner for providing information on current and future radiometer capabilities. C. Naudet and S. Keihm made a number of useful suggestions after reading an early draft of this article.

References

[1] M. Tinto and J. W. Armstrong, "Spacecraft Doppler Tracking as a Narrow-Band Detector of Gravitational Radiation," *Phys. Rev. D*, vol. 58, article 042002, 1998.

[2] A. E. E. Rogers, A. T. Moffet, D. C. Backer, and J. M. Moran, "Coherence Limits in VLBI Observations at 3-mm Wavelength," *Radio Sci.*, vol. 19, pp. 1552–1560, 1984.

[3] R. J. Hill, R. S. Lawrence, and J. T. Priestly, "Theoretical and Calculational Aspects of the Radio Refractive Index of Water Vapor," *Radio Sci.*, vol. 17, pp. 1251–1257, 1982.

[4] J. C. Owens, "Optical Refractive Index of Air: Dependence on Pressure, Temperature, and Composition," *Applied Optics*, vol. 6, pp. 51–58, 1967.

[5] G. Elgered, "Tropospheric Radio Path Delay From Ground-Based Microwave Radiometry," Chapter 5, *Atmospheric Remote Sensing by Microwave Radiometry*, edited by M. Janssen, New York: John Wiley, 1993.

[6] G. M. Resch, D. E. Hogg, and P. J. Napier, "Radiometric Correction of Atmospheric Path Length Fluctuations in Interferometric Experiments," *Radio Sci.*, vol. 19, pp. 411-422, January 1984.

[7] A. B. Tanner, "Development of a High-Stability Water Vapor Radiometer," *Radio Sci.*, vol. 33, pp. 449–462, March 1998.

[8] S. J. Keihm and K. A. Marsh, "Advanced Algorithm and System Development for Cassini Radio Science Troposphere Calibration," *The Telecommunications and Data Acquisition Progress Report 42-127, July–September 1996*, Jet Propulsion Laboratory, Pasadena, California, pp. 1–20, November 15, 1996.
http://tmo.jpl.nasa.gov/tmo/progress_report/42-127/127A.pdf

[9] C. Naudet, C. Jacobs, S. Keihm, G. Lanyi, R. Linfield, G. Resch, L. Riley, H. Rosenberger, and A. Tanner, "The Media Calibration System for Cassini Radio Science: Part I," *The Telecommunications and Mission Operations Progress Report 42-143, July–September 2000*, Jet Propulsion Laboratory, Pasadena, California, pp. 1–8, November 15, 2000.
http://tmo.jpl.nasa.gov/tmo/progress_report/42-143/143I.pdf

[10] R. P. Linfield and J. Z. Wilcox, "Radio Metric Errors Due to Mismatch and Offset Between a DSN Antenna Beam and the Beam of a Troposphere Calibration Instrument," *The Telecommunications and Data Acquisition Progress Report 42-114, April–June, 1993*, Jet Propulsion Laboratory, Pasadena, California, pp. 1–13, August 15, 1993.
http://tmo.jpl.nasa.gov/tmo/progress_report/42-114/114A.pdf

[11] A. B. Tanner, "Embedding a Water Vapor Radiometer in a DSN Antenna: Experimental Results from DSS 13," *The Telecommunications and Mission Operations Progress Report 42-143, July–September 2000*, Jet Propulsion Laboratory, Pasadena, California, pp. 1–23, November 15, 2000.
http://tmo.jpl.nasa.gov/tmo/progress_report/42-143/143M.pdf

[12] R. N. Treuhaft and G. E. Lanyi, "The Effect of the Dynamic Wet Troposphere on Radio Interferometric Measurements," *Radio Science*, vol. 22, no. 2, pp. 251–265, 1987.

[13] R. P. Linfield, "Effect of Aperture Averaging upon Tropospheric Phase Fluctuations Seen with a Radio Antenna," *Radio Sci.*, vol. 33, pp. 1353–1359, September 1998.

[14] D. W. Allan, "Statistics of Atomic Frequency Standards," *Proc. IEEE*, vol. 54, no. 2, pp. 221–230, 1966.

[15] A. R. Thompson, J. M. Moran, and G. W. Swenson, Jr., *Interferometry and Synthesis in Radio Astronomy*, New York: John Wiley, pp. 277-278, 1986.

[16] R. P. Linfield, M. M. Colavita, and B. F. Lane, "Atmospheric Turbulence Measurements with the Palomar Testbed Interferometer," *The Astrophysical Journal*, vol. 553, 2001 (in press).